Numerical Simulation and Analysis of Annular Trapped Pressure during the Testing of Deepwater High-Temperature and High-Pressure Gas Wells

Zhihua Rao[1,2], Kunxiang Liu[1,2], Bin Chen[2], Yao You[2], Qiang Zhang[2], Yang Jiao[2], Baobo Liu[2] and Miao He[3,*]

[1] National Key Laboratory of Offshore Oil and Gas Exploitation, Beijing, 102209, China

[2] Shenzhen Branch of CNOOC (China) Co., Ltd., Shenzhen, 518067, China

[3] School of Petroleum Engineering, Yangtze University, Wuhan, 430100, China

Revista Internacional
Métodos numéricos
para cálculo y diseño en ingeniería
RIMNI
UNIVERSITAT POLITÈCNICA DE CATALUNYA BARCELONATECH
In cooperation with CIMNE

INFORMATION

Keywords:
Annular temperature
annular volume
annular trapped pressure
pressure prediction
high temperature and high pressure

DOI: 10.23967/j.rimni.2025.10.72796

SCIPEDIA Revista Internacional de Métodos Numéricos para Cálculo y Diseño en Ingeniería

Revista Internacional Métodos numéricos para cálculo y diseño en ingeniería RIMNI

In cooperation with CIMNE

Numerical Simulation and Analysis of Annular Trapped Pressure during the Testing of Deepwater High-Temperature and High-Pressure Gas Wells

Zhihua Rao[1,2], Kunxiang Liu[1,2], Bin Chen[2], Yao You[2], Qiang Zhang[2], Yang Jiao[2], Baobo Liu[2] and Miao He[3,*]

[1]National Key Laboratory of Offshore Oil and Gas Exploitation, Beijing, 102209, China

[2]Shenzhen Branch of CNOOC (China) Co., Ltd., Shenzhen, 518067, China

[3]School of Petroleum Engineering, Yangtze University, Wuhan, 430100, China

ABSTRACT

During the testing of high-temperature and high-pressure (HTHP) offshore gas wells, heat transfer occurs between the high-temperature gas in the tubing and the low-temperature fluid in the annulus. This causes the annular fluid to expand, leading to an increase in annular trapped pressure, which poses a potential integrity risk. To accurately predict this pressure variation, a full-scale physical model of an offshore HTHP gas well was developed based on simplified assumptions of a constant geothermal gradient and homogeneous casing material. By integrating the Pressure–Volume–Temperature (PVT) equation of state with a transient heat transfer model of the wellbore, a section-by-section method for calculating annular temperature was proposed. A coupled prediction model for annular trapped pressure, incorporating both thermal effects and annular volume change, was then established. Using Well Y in the eastern South China Sea as a case study, numerical simulations of annular temperature and trapped pressure were performed. The results indicate that the model's average relative error compared to experimental data is approximately 6.15%. When the production rate is 10×10^4 m^3/d, the trapped pressures in annuli A, B, and C are 31, 25, and 21 MPa, respectively. Both temperature and pressure increase progressively from the wellhead to the bottom, with the most significant variations occurring in the shallow section. Sensitivity analysis shows that trapped pressure rises rapidly during the early stage of testing and gradually levels off over time. The annular trapped pressure is positively correlated with production rate, geothermal gradient, fluid expansion coefficient, and well depth, whereas increases in casing elastic modulus, Poisson's ratio, and the thermal expansion coefficient of the fluid tend to reduce it. The study provides a theoretical foundation and practical support for evaluating wellbore integrity and controlling annular risks under complex conditions in deep-water HTHP oil and gas wells.

OPEN ACCESS

Received: 03/09/2025

Accepted: 11/11/2025

Published: 16/04/2026

DOI
10.23967/j.rimni.2025.10.72796

Keywords:
Annular temperature
annular volume
annular trapped pressure
pressure prediction
high temperature and high pressure

*Correspondence: Miao He (hemiao@yangtzeu.edu.cn).

1 Introduction

During the testing and development of high-temperature and high-pressure oil and gas wells, the temperature difference of the wellbore fluid under static and dynamic conditions can cause thermal expansion and generate thermal stress. During the testing period of oil and gas wells, the temperature difference between the tubing and the annulus causes the temperature in the annulus to rise rapidly. The liquid in the annulus expands due to heat, and the limited annulus space cannot accommodate the expanded volume, resulting in annular trapped pressure [1,2]. When the trapped pressure exceeds the strength limit of the casing, it may cause casing damage or push the wellhead upward, damaging the wellbore integrity. Studying and predicting the variation law of annular trapped pressure can effectively prevent the increase of annular trapped pressure, which is of great significance for ensuring the safe and efficient production of deep-sea oil and gas wells [3,4].

The stratification of annular pressure is influenced by multiple factors, primarily including the following: First, thermal expansion of the annular liquid due to heating; Second, deformation of the inner and outer walls of the casing string, which alters the volume of the annular space; Third, fluid loss from the annulus, invasion of high-pressure formation gas into the annular space, or failure of the cement sheath's sealing integrity [5–8].

In recent years, researchers worldwide have undertaken extensive studies on predicting annular trapped pressure, proposing a range of methods and models to elucidate the governing patterns of annular pressure fluctuations. Existing research can be broadly categorized into four major directions:

(1) Thermo-mechanical coupling models

These studies focus on the mechanism of annular trapped pressure caused by thermally induced expansion, and they typically couple temperature changes with casing deformation to evaluate annular volume variation. Iterative algorithms and elastic deformation theory are employed to simulate transient heat and pressure responses. For instance, numerical methods have been developed to analyze wellbore temperature and pressure variation over time, revealing that annular temperature and pressure rise rapidly during the early production stage and then stabilize gradually, with strong correlation to the geothermal gradient [9]. In deepwater wells, casing deformation was incorporated into predictive models to reduce error margins, enhancing safety in wellbore design [10]. Nonlinear variations in fluid temperature and pressure properties were also introduced to improve the accuracy of annular trapped pressure predictions under realistic thermodynamic behavior [11].

(2) Multiphase and seepage-based transient models

Another group of studies addresses more complex fluid behaviors, such as multiphase flow, nitrogen injection, and formation fluid invasion. These models often emphasize unsteady-state processes and account for fluid exchange between annuli and formations. For example, two-phase and multicomponent flow theories were used to simulate pressure behavior during nitrogen injection, confirming that partial gas slugs can alleviate thermal annular pressure buildup in annulus A [12]. Other work developed transient mathematical models for annular pressure buildup during staged fracturing, factoring in the seepage of formation fluids [13]. Further, annular pressure buildup under seepage conditions and solid phase deposition in annular fluids has been addressed through predictive analysis based on permeability and deposition characteristics [14].

(3) Data-driven modeling approaches

Recent developments include the application of machine learning and regression models to enhance prediction performance. These approaches leverage experimental pressure–volume–temperature (PVT) data to establish relationships such as fluid density as a function of temperature

and pressure, enabling better design of annular fluids and casings for annular pressure buildup mitigation [15].

(4) Integrated physical models and field validation

A number of studies aim to combine multiple physical effects—such as tubing leakage, thermal transmission across multiple annuli, and wellbore-formation interaction—into unified models. These works often involve experimental measurements and field data for parameter calibration and model verification. One such model accounts for tubing leakage and coupled annular behavior to simulate annular trapped pressure accumulation, integrating wellbore temperature profiles and thermodynamic properties of annular fluids [16].

Collectively, these research efforts have provided significant insights into the mechanisms and influencing factors of annular trapped pressure and annular pressure buildup.

Although existing methods have partially elucidated the patterns of pressure variation within the annulus, they still exhibit notable limitations. First, the majority of approaches rely on steady-state models to calculate annular temperature, thereby neglecting the coupling effects among multiple annuli. This simplification often results in reduced accuracy in estimating both temperature distribution and volume changes. Second, there is a lack of systematic theoretical investigation into annular pressure buildup induced by thermal expansion. Current research seldom addresses the complex thermal interactions and volumetric variations occurring between different annuli. Furthermore, existing models provide insufficient analysis of the nonlinear effects of key sensitive parameters—such as test production, geothermal gradients, and casing properties—on annular temperature and trapped pressure. These omissions contribute to the low predictive accuracy of current models.

To more accurately predict annular confining pressure and analyze its variation patterns, this study develops a full-scale physical model of deepwater high-temperature and high-pressure (HTHP) gas wells. The model incorporates actual wellbore structural parameters, including geometric dimensions, casing properties, material characteristics, and the geometric and physical features of multiple annuli. It should be noted that this physical model is not an experimental apparatus but a numerical simulation framework constructed based on real wellbore configurations. Building on this framework, and integrating the principles of wellbore thermodynamics and volume compatibility, a section-by-section annular temperature calculation model is established. Furthermore, a deepwater HTHP annular trapped pressure prediction model is developed, coupling thermal effects with annular volume variations.

Using field data from the HTHP Y well in the eastern South China Sea, numerical simulations are conducted to investigate the temperature and trapped pressure distributions in different annuli. A sensitivity analysis is also performed to examine the influence of testing time, production rate, geothermal gradient, and casing properties. The objective of this study is to establish a comprehensive modeling framework that enhances the accuracy of annular trapped pressure prediction and provides theoretical guidance for pressure control, wellbore integrity design, and the safe, efficient development of deepwater HTHP gas wells.

2 Model Establishment

2.1 Annular Temperature Control Equation

Offshore high-temperature and high-pressure (HTHP) gas wells commonly utilize subsea Christmas trees, wherein the wellbore is situated below the mudline in a sealed condition. This configuration effectively isolates the wellbore from external fluctuations in seawater and seabed pressure. During

well testing, heat transfer occurs between the high-temperature, high-pressure gas flowing from the bottom hole to the wellhead and the surrounding geological formations at corresponding depths [17]. The term annulus refers to the uncemented space between two concentric casing strings. Specifically, the space between the tubing and the production casing is referred to as Annulus A; that between the production casing and the technical casing is defined as Annulus B; and the space between the technical casing and the surface casing is designated as Annulus C [18,19]. A schematic representation of the physical model for an offshore HTHP oil and gas well is provided in Fig. 1.

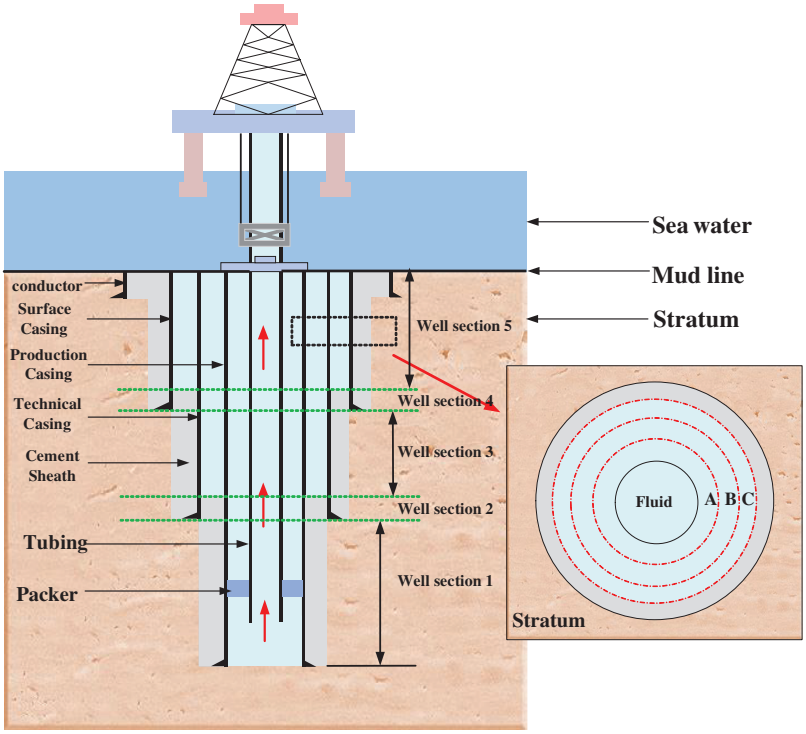

Figure 1: Physical model of offshore high-temperature and high-pressure oil and gas wells

In order to simplify the analysis and calculation, the following assumptions are made based on the API 17D standard and the API 5CT standard:

(1) The annuli are completely filled with test fluid and maintain perfect sealing integrity. This is ensured by subsea Christmas trees conforming to API 17D standards and packer/cementing operations that isolate the annuli from external communication.

(2) The model considers only the deformation of the inner casing. The inner casing directly experiences wellbore pressure and temperature changes, contributing most to annular volume variation.

(3) The casing materials are homogeneous, and their thermophysical properties remain constant over time and are unaffected by temperature variations. API 5CT specifications ensure uniform mechanical and chemical properties over the casing length.

(4) During testing, the geothermal gradient is constant with depth and is known in advance. Short-term testing in deepwater wells generally exhibits a stable geothermal gradient, which can be obtained from well logging data.

(5) At the same depth, the temperature variations of the test fluids are identical across all annuli. Radial temperature differences are negligible over short time scales under similar formation contact conditions.

(6) Heat transfer from the tubing to the outer diameter of the cement sheath is assumed to be steady-state, whereas heat transfer from the outer diameter of the cement sheath to the surrounding formation is considered transient. The inner path is short and thermally stable, while the outer path involves time-dependent heat diffusion in the formation.

It should be emphasized that the above assumptions represent idealized simplifications of actual wellbore conditions. In real high-temperature and high-pressure gas wells, complete annular sealing may be compromised by micro-annuli or minor cement defects, leading to limited fluid migration or partial pressure dissipation between annuli. The geothermal gradient may also vary locally due to differences in lithology, formation fluid movement, or transient thermal effects, deviating from the assumed constant profile.

In addition, casing materials may not exhibit perfectly homogeneous mechanical and thermal properties, and their elastic modulus and thermal expansion coefficients can change slightly with temperature. The assumption of steady-state heat transfer within the inner annulus may likewise be oversimplified under conditions of rapid temperature fluctuations. These factors may cause deviations between the modeled and actual annular pressure responses, and should be carefully considered when interpreting the model's applicability to field operations.

2.1.1 Energy Equation

In offshore high-temperature and high-pressure (HTHP) gas wells, multiple annuli exist within the wellbore during testing, with their number varying across different well sections. This structural variability leads to distinct heat transfer behaviors along the well. To address this complexity, the present study develops a temperature prediction model for each annulus within individual well sections, enabling accurate estimation of temperature variations. During the testing and production phases, precisely quantifying the heat loss from the high-temperature gas in the tubing to the surrounding low-temperature formations is critical for reliable calculation of annular temperatures.

A annulus serves as a barrier between the tubing and the production casing and is filled with test fluid during the testing period. The annular trapped pressure in A annulus is influenced by volumetric changes of the tubing and production casing strings.

According to the physical model of the offshore high-temperature and high-pressure gas well shown in Fig. 1, the radial total thermal resistance of the first part of the well section and the thermal resistance from the calculation point of the A annulus to the outer edge of the adjacent cement sheath are, respectively:

$$\begin{cases} R_{to1} = \dfrac{1}{\pi d_1 h} + \dfrac{1}{2\pi\lambda_a}\ln\dfrac{d_2}{d_1} + \dfrac{1}{2\pi\lambda_{ce}}\ln\dfrac{d_3}{d_2} \\ R_{zro\_a1} = \dfrac{1}{2\pi\lambda_a}\ln\dfrac{d_2}{d_1} + \dfrac{1}{2\pi\lambda_{ce}}\ln\dfrac{d_3}{d_2} \end{cases} \tag{1}$$

where, R_{to1} is the total thermal resistance for radial heat transfer when considering well section 1, (m·°C)/W; d_1 represents the diameter of the tubing, m; d_2 represents the diameter of the production casing, m; d_3 represents the diameter of the technical casing, m; h represents the convective heat transfer coefficient, W/(m^2·°C); λ_a represents the thermal conductivity of the test fluid within the cavity of

the A annulus, W/(m·°C); λ_{ce} represents the thermal conductivity of the cement sheath test solution, W/(m·°C); R_{zro_a1} represents the thermal resistance from the inner surface of the A annulus to the outer edge of the cement sheath, (m·°C)/W.

Zhang B et al., based on the semi-steady state wellbore temperature calculation model, proposed a wellbore annulus temperature calculation model for deepwater oil and gas well production [9,20]. The temperature calculation equation for A annulus is expressed as follows:

$$T_{\mathrm{a1}(z,r,t)} = T_{\mathrm{ce1}} + \frac{R_{\mathrm{zro\_a1}}}{R_{\mathrm{to1}}}\left(T_{\mathrm{p1}} - T_{\mathrm{ce1}}\right) \tag{2}$$

where, T_{a1} is the temperature of the A annulus in the well section 1, °C; T_{ce1} is the temperature of the outer boundary of the cement sheath in well section 1, °C; T_{p1} is the temperature inside the tubing in well section 1, °C.

section 2 lies between the cement return height of B annulus and the shoe depth of the technical casing. At this stage, the annular temperature of section 2 is influenced by the cemented section below C annulus. The radial total thermal resistance of well section 2 and the total thermal resistance from the calculation point in the annulus to the outer edge of the cement sheath are:

$$\begin{cases} R_{to2} = \dfrac{1}{\pi d_1 h} + \dfrac{1}{2\pi\lambda_{\mathrm{a}}}\ln\dfrac{d_2}{d_1} + \dfrac{1}{2\pi\lambda_{\mathrm{ce}}}\ln\dfrac{d_3}{d_2} + \dfrac{1}{2\pi\lambda_{\mathrm{ce}}}\ln\dfrac{d_4}{d_3} \\ R_{zro\_a2} = \dfrac{1}{2\pi\lambda_{\mathrm{a}}}\ln\dfrac{d_2}{d_1} + \dfrac{1}{2\pi\lambda_{\mathrm{a}}}\ln\dfrac{d_3}{d_2} + \dfrac{1}{2\pi\lambda_{\mathrm{ce}}}\ln\dfrac{d_4}{d_3} \end{cases} \tag{3}$$

where, R_{to2} is the total thermal resistance for radial heat transfer when considering the well section 2, (m·°C)/W; d_4 represents the diameter of the surface casing, m; R_{zro_a2} is the thermal resistance calculated within the A annulus from the calculation point to the outer edge of the cement sheath when considering the well section 2, (m·°C)/W.

When considering section 2, the annular temperature in A annulus is expressed as:

$$T_{\mathrm{a2}(z,r,t)} = T_{\mathrm{ce2}} + \frac{R_{\mathrm{zro\_a2}}}{R_{\mathrm{to2}}}\left(T_{\mathrm{p2}} - T_{\mathrm{ce2}}\right) \tag{4}$$

where, T_{a2} is the temperature of the A annulus in the well section 2, °C; T_{ce2} is the temperature of the outer boundary of the cement sheath in well section 2, °C; T_{p2} is the temperature inside the tubing in well section 2, °C.

section 3 lies between the cement return heights of B annulus and C annulus. At this stage, section 3 includes both A annulus and B annulus, and the temperature in B annulus is influenced by the outermost cement sheath. At this point, when considering well section 3, the radial total thermal resistances of the A annulus and the B annulus, as well as the total thermal resistances of the annulus calculation points to the outer edge of the cement sheath, are as follows:

$$\begin{cases} R_{to3} = \dfrac{1}{\pi d_1 h} + \dfrac{1}{2\pi\lambda_{\mathrm{a}}}\ln\dfrac{d_2}{d_1} + \dfrac{1}{2\pi\lambda_{\mathrm{ce}}}\ln\dfrac{d_3}{d_2} + \dfrac{1}{2\pi\lambda_{\mathrm{ce}}}\ln\dfrac{d_4}{d_3} \\ R_{zro\_a3} = \dfrac{1}{2\pi\lambda_{\mathrm{a}}}\ln\dfrac{d_2}{d_1} + \dfrac{1}{2\pi\lambda_{\mathrm{b}}}\ln\dfrac{d_3}{d_2} + \dfrac{1}{2\pi\lambda_{\mathrm{ce}}}\ln\dfrac{d_4}{d_3} \\ R_{zro\_b3} = \dfrac{1}{2\pi\lambda_{\mathrm{b}}}\ln\dfrac{d_3}{d_2} + \dfrac{1}{2\pi\lambda_{\mathrm{ce}}}\ln\dfrac{d_4}{d_3} + \dfrac{1}{2\pi\lambda_{\mathrm{ce}}}\ln\dfrac{d_5}{d_4} \end{cases} \tag{5}$$

where, R_{to3} represents the total thermal resistance for radial heat transfer when considering the well section 3, (m·°C)/W; d_5 is the diameter of the conductor, m; R_{zro_a3} represents the thermal resistance from the calculation point within the A annulus to the outer edge of the cement sheath when considering the well section 3, (m·°C)/W; R_{zro_b3} is the thermal resistance from the calculation point within the B annulus to the outer edge of the cement ring when considering the well section 3, (m·°C)/W; λ_b represents the thermal conductivity of the test fluid within the cavity of the B annulus, W/(m·°C).

When considering section 3, the temperatures in A annulus and B annulus are expressed as:

$$\begin{cases} T_{\mathrm{a3}(z,r,t)} = T_{\mathrm{ce3}} + \dfrac{R_{\mathrm{zro\_a3}}}{R_{\mathrm{to3}}}\left(T_{\mathrm{p3}} - T_{\mathrm{ce3}}\right) \\ T_{\mathrm{b3}(z,r,t)} = T_{\mathrm{ce3}} + \dfrac{R_{\mathrm{zro\_b3}}}{R_{\mathrm{to3}}}\left(T_{\mathrm{p3}} - T_{\mathrm{ce3}}\right) \end{cases} \tag{6}$$

where, T_{a3} is the temperature of the A annulus in the well section 3, °C; T_{ce3} is the temperature of the outer boundary of the cement sheath in well section 3, °C; T_{p3} is the temperature inside the tubing in well section 3, °C; T_{b3} is the temperature of the B annulus in the well section 3, °C.

section 4 lies between the cement return height of C annulus and the depth of the outermost cement sheath. At this stage, section 4 includes A annulus, B annulus, and C annulus, and the temperatures in B annulus and C annulus are influenced by the outermost cement sheath. When considering the well section 4, the radial total thermal resistances of the A annulus, B annulus and C annulus, as well as the total thermal resistances from the calculation points of the annulus to the outer edge of the cement ring, are, respectively:

$$\begin{cases} R_{to4} = \dfrac{1}{\pi d_1 h} + \dfrac{1}{2\pi\lambda_{\mathrm{a}}}\ln\dfrac{d_2}{d_1} + \dfrac{1}{2\pi\lambda_{\mathrm{ce}}}\ln\dfrac{d_3}{d_2} + \dfrac{1}{2\pi\lambda_{\mathrm{c}}}\ln\dfrac{d_4}{d_3} \\ R_{zro\_\mathrm{a4}} = \dfrac{1}{2\pi\lambda_{\mathrm{a}}}\ln\dfrac{d_2}{d_1} + \dfrac{1}{2\pi\lambda_{\mathrm{b}}}\ln\dfrac{d_3}{d_2} + \dfrac{1}{2\pi\lambda_{\mathrm{ce}}}\ln\dfrac{d_4}{d_3} \\ R_{zro\_\mathrm{b4}} = \dfrac{1}{2\pi\lambda_{\mathrm{b}}}\ln\dfrac{d_3}{d_2} + \dfrac{1}{2\pi\lambda_{\mathrm{c}}}\ln\dfrac{d_4}{d_3} + \dfrac{1}{2\pi\lambda_{\mathrm{ce}}}\ln\dfrac{d_5}{d_4} \\ R_{zro\_\mathrm{c4}} = \dfrac{1}{2\pi\lambda_{\mathrm{c}}}\ln\dfrac{d_4}{d_3} + \dfrac{1}{2\pi\lambda_{\mathrm{ce}}}\ln\dfrac{d_5}{d_4} \end{cases} \tag{7}$$

where, R_{to4} represents the total thermal resistance for radial heat transfer when considering the well section 4, (m·°C)/W; R_{zro_a4} is the thermal resistance from the calculation point in the A annulus to the outer diameter of the cement ring, (m·°C)/W; R_{zro_b4} is the thermal resistance from the calculation point in the B annulus to the outer edge of the cement ring, (m·°C)/W; R_{zro_c4} is the thermal resistance from the calculation point in the C annulus to the outer edge of the cement ring, (m·°C)/W; λ_c is the thermal conductivity of the test fluid in the C annulus, W/(m·°C).

When considering section 4, the temperatures in A annulus, B annulus, and C annulus are expressed as:

$$\begin{cases} T_{\mathrm{a4}(z,r,t)} = T_{\mathrm{ce4}} + \dfrac{R_{\mathrm{zro\_a4}}}{R_{\mathrm{to4}}}\left(T_{\mathrm{p4}} - T_{\mathrm{ce4}}\right) \\ T_{\mathrm{b4}(z,r,t)} = T_{\mathrm{ce4}} + \dfrac{R_{\mathrm{zro\_b4}}}{R_{\mathrm{to4}}}\left(T_{\mathrm{p4}} - T_{\mathrm{ce4}}\right) \\ T_{\mathrm{c4}(z,r,t)} = T_{\mathrm{ce4}} + \dfrac{R_{\mathrm{zro\_c4}}}{R_{\mathrm{to4}}}\left(T_{\mathrm{p4}} - T_{\mathrm{ce4}}\right) \end{cases} \tag{8}$$

where, T_{a4} is the temperature of the A annulus in the well section 4, °C; T_{ce4} is the temperature of the outer boundary of the cement sheath in well section 4, °C; T_{p4} is the temperature inside the tubing in well section 4, °C; T_{b4} is the temperature of the B annulus in the well section 4, °C; T_{c4} is the temperature of the C annulus in the well section 4, °C.

The depth of section 5 corresponds to the depth of the outermost cement sheath. At this stage, section 5 includes A annulus, B annulus, and C annulus, and the temperatures in A annulus, B annulus, and C annulus are all influenced by the outermost cement sheath. When considering the well section 5, the radial total thermal resistances of the A annulus, B annulus and C annulus, as well as the total thermal resistances from the calculation points of the annulus to the outer edge of the cement ring, are, respectively:

$$\begin{cases} R_{to5} = \dfrac{1}{\pi d_1 h} + \dfrac{1}{2\pi\lambda_{\mathrm{a}}}\ln\dfrac{d_2}{d_1} + \dfrac{1}{2\pi\lambda_{\mathrm{ce}}}\ln\dfrac{d_3}{d_2} + \dfrac{1}{2\pi\lambda_{\mathrm{c}}}\ln\dfrac{d_4}{d_3} + \dfrac{1}{2\pi\lambda_{\mathrm{ce}}}\ln\dfrac{d_5}{d_4} \\ R_{zro\_\mathrm{a5}} = \dfrac{1}{2\pi\lambda_{\mathrm{a}}}\ln\dfrac{d_2}{d_1} + \dfrac{1}{2\pi\lambda_{\mathrm{b}}}\ln\dfrac{d_3}{d_2} + \dfrac{1}{2\pi\lambda_{\mathrm{c}}}\ln\dfrac{d_4}{d_3} + \dfrac{1}{2\pi\lambda_{\mathrm{ce}}}\ln\dfrac{d_5}{d_4} \\ R_{zro\_\mathrm{b5}} = \dfrac{1}{2\pi\lambda_{\mathrm{b}}}\ln\dfrac{d_3}{d_2} + \dfrac{1}{2\pi\lambda_{\mathrm{c}}}\ln\dfrac{d_4}{d_3} + \dfrac{1}{2\pi\lambda_{\mathrm{ce}}}\ln\dfrac{d_5}{d_4} \\ R_{zro\_\mathrm{c5}} = \dfrac{1}{2\pi\lambda_{\mathrm{c}}}\ln\dfrac{d_4}{d_3} + \dfrac{1}{2\pi\lambda_{\mathrm{ce}}}\ln\dfrac{d_5}{d_4} \end{cases} \tag{9}$$

where, R_{to5} represents the total thermal resistance for radial heat transfer when considering the well section 5, (m·°C)/W; R_{zro_a5} is the thermal resistance from the calculation point in the A annulus to the outer diameter of the cement ring, (m·°C)/W; R_{zro_b5} is the thermal resistance from the calculation point in the B annulus to the outer edge of the cement ring, (m·°C)/W; R_{zro_c5} is the thermal resistance from the calculation point in the C annulus to the outer edge of the cement ring, (m·°C)/W.

When considering section 5, the temperatures in A annulus, B annulus, and C annulus are expressed as:

$$\begin{cases} T_{\mathrm{a5}(z,r,t)} = T_{\mathrm{ce5}} + \dfrac{R_{\mathrm{zro\_a5}}}{R_{\mathrm{to4}}}\left(T_{\mathrm{p5}} - T_{\mathrm{ce5}}\right) \\ T_{\mathrm{b5}(z,r,t)} = T_{\mathrm{ce5}} + \dfrac{R_{\mathrm{zro\_b5}}}{R_{\mathrm{to5}}}\left(T_{\mathrm{p5}} - T_{\mathrm{ce5}}\right) \\ T_{\mathrm{c5}(z,r,t)} = T_{\mathrm{ce5}} + \dfrac{R_{\mathrm{zro\_c5}}}{R_{\mathrm{to5}}}\left(T_{\mathrm{p5}} - T_{\mathrm{ce5}}\right) \end{cases} \tag{10}$$

where, T_{a5} is the temperature of the A annulus in the well section 5, °C; T_{ce5} is the temperature of the outer boundary of the cement sheath in well section 5, °C; T_{p5} is the temperature inside the tubing in

well section 5, °C; T_{b5} is the temperature of the B annulus in the well section 5, °C; T_{c5} is the temperature of the C annulus in the well section 5, °C.

Fig. 2 shows the iterative solution process of the coupled temperature–pressure model. The model solves the temperature and pressure of the tubing, cement ring and each annular space within the wellbore through iterative calculations. Firstly, the wellbore structure and physical property parameters are input, and the initial temperature and pressure are set. Then, the radial thermal resistance is calculated and the temperature is solved layer by layer. After correction using the geothermal gradient and time function, the volume changes caused by the thermal expansion and compression of the casing and the fluid are calculated. The annular trapped pressure is updated through the volume compatibility equation until the temperature and pressure converge simultaneously.

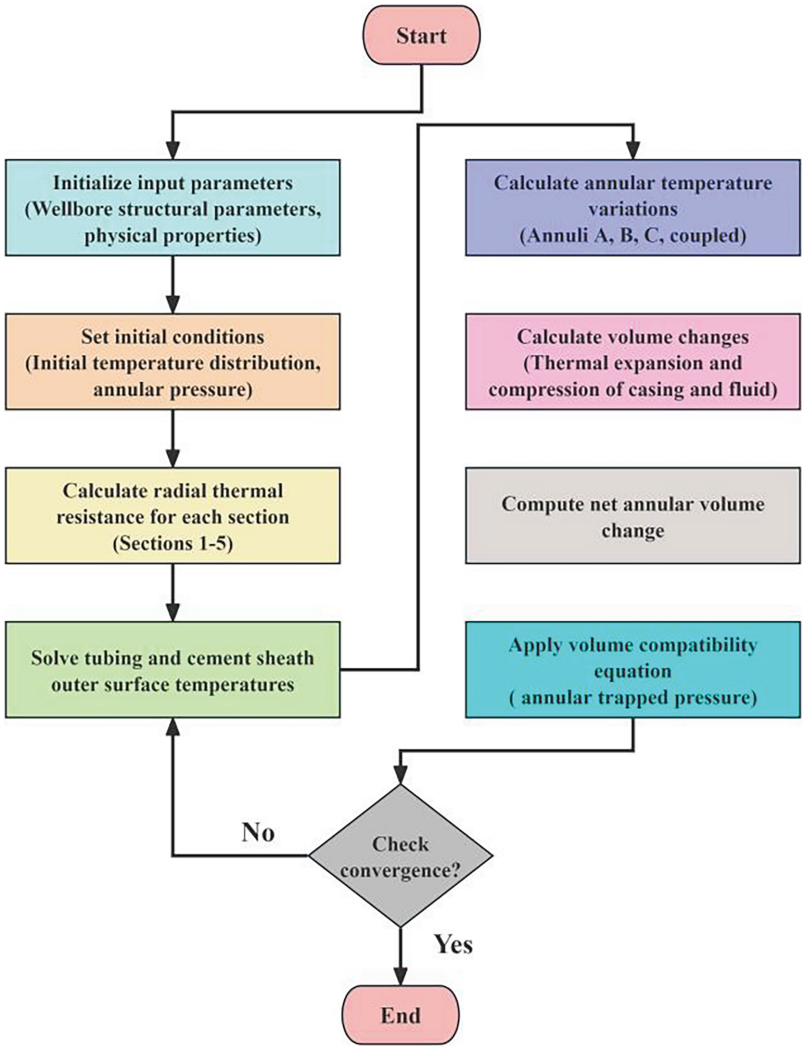

Figure 2: Iterative solution flowchart of the model

2.1.2 Auxiliary Equation

In Eq. (2), T_p represents the temperature of the reservoir fluid inside the tubing. Depending on the well section, the temperature varies at different positions within the tubing. The temperature is calculated using the following formula:

$$T_{\mathrm{p}}(z,t) = T_b + G_{\mathrm{T}}(A - z) - Ce^{-z/A} \tag{11}$$

where, G_T is geothermal gradient, °C/m; T_b is bottom hole temperature, °C; A is a calculation parameter and has no actual physical meaning, z is the distance from the calculation point to the bottom of the well, m; C is the specific heat capacity, J/(Kg·°C).

The temperature at the outer boundary of the cement sheath is influenced by the total radial thermal resistance from the calculation point to the boundary of the cement sheath, as well as by the stratum temperature and the thermal conductivity of the stratum. The calculation formula is as follows:

$$T_{\mathrm{c}} = \frac{t_D T_r + 2\pi\lambda_{\mathrm{f}} R_{\mathrm{to}} T_{\mathrm{f}}}{t_D + 2\pi\lambda_{\mathrm{f}} R_{\mathrm{to}}} \tag{12}$$

where, T_c is the temperature from the calculation point to the outer boundary of the cement sheath, °C; t_D is dimensionless production time, λ_f is the thermal conductivity of the stratum, W/(m·°C); T_r is the temperature of the calculation point, °C; R_{to} is the total thermal resistance for radial heat transfer, m·°C/W; T_f is the temperature of stratum, °C.

The dimensionless time function adopts the Hasan formula [21]:

$$f(t_D)\begin{cases} 1.1281 t_D{}^{1/2}\left(1 - 0.3 t_D{}^{1/2}\right), \left(10^{-10} \le t_D \le 1.5\right) \\ (0.4063 + 0.5\ln t_D)\left(1 + \frac{0.6}{t_D}\right), (t_D > 1.5) \end{cases} \tag{13}$$

Among them, the calculation formula for t_D is:

$$t_D = \frac{\alpha_{\mathrm{f}} t}{r_{\mathrm{w}}^2} \tag{14}$$

where, t is time, s; α_f is the diffusion coefficients of stratum, m²/s; r_w is the well hole radius, m.

A is a calculation parameter and does not have any actual physical meaning. The specific calculation method is as follows [22]:

$$A = \frac{Q_{\mathrm{f}} C_{\mathrm{f}} (t_D + 2\pi\lambda_{\mathrm{f}} R_{\mathrm{to}})}{2\pi\lambda_{\mathrm{f}}} \tag{15}$$

where, Q_f is the mass flow rate of reservoir fluid, kg/s; C_f is the specific heat capacity of reservoir fluid, J/(kg·°C).

2.2 Annular Trapped Pressure Control Equation

In the study of annular trapped pressure, the space between casing strings can be treated as a sealed container filled with fluid. A schematic of the annular volume variation is shown in Fig. 3. This paper focuses on the annular pressure buildup resulting from thermal effects. When the temperature of the annular fluid increases due to heating, its volume tends to expand. However, the rigid structure of the wellbore restricts this expansion. As a result, the heated fluid exerts pressure on the inner wall of the annular space—this is referred to as annular trapped pressure [23,24].

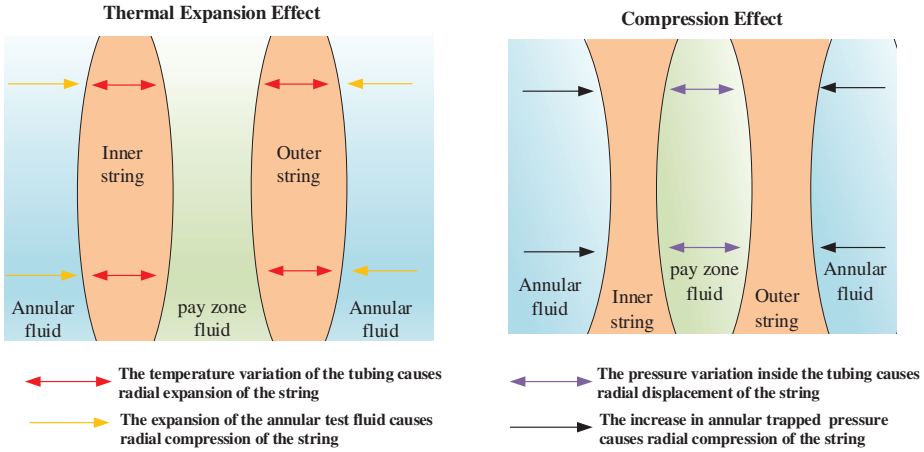

Figure 3: Wellbore volume variation schematic diagram

According to Newton's third law, the container wall applies an equal and opposite force to resist the expansion of the fluid. This compressive resistance prevents free expansion and leads to a rise in pressure within the annulus. Therefore, as long as the structural integrity of the casing system is maintained, the increase in annular trapped pressure is primarily governed by the thermal expansion properties of the fluid and the degree of volume change within the annular space.

The annular trapped pressure induced by thermal effects is analogous to the "aquathermal pressuring" phenomenon observed in petroleum geology. When the annulus between casings is treated as a closed system, heat transfer into the annular space causes simultaneous changes in both the volume of the annular fluid and the annular geometry. However, due to the significant differences in thermal properties between the annular test fluid and the casing materials, the confined annular space cannot readily accommodate the thermally expanded fluid. According to the principle of volume compatibility, the resulting annular trapped pressure exerts a reactive force on the fluid to counterbalance the volume increase caused by thermal expansion.

Since the annulus is sealed, the annular volume and the volume of the annular test fluid remain equal throughout the testing process in high-temperature and high-pressure gas wells. This phenomenon can be summarized as [25,26]:

$$\Delta V_{\mathrm{vt}} - \Delta V_{\mathrm{vp}} = \Delta V_{\mathrm{a}} \tag{16}$$

where, ΔV_{vt} is the volume change of the annular test fluid caused by thermal expansion, m^3; ΔV_{vp} is the volume change of the test fluid in the annulus during annular pressure increase, m^3; ΔV_a is The change in annular volume, m^3.

When the annular test fluid is heated and expands, its volume change is related to its isobaric expansion coefficient. As the annular pressure increases, the annular test fluid is compressed and the change of the volume of the annular test fluid is related to its isothermal compression coefficient. The volume change due to thermal expansion and the volume change due to pressure compression are expressed as follows:

$$\begin{cases} \Delta V_{\mathrm{vt}} = \alpha V_v \Delta T \\ \Delta V_{\mathrm{vp}} = k V_v \Delta p \end{cases} \tag{17}$$

where, α is the isobaric expansion coefficient of the annular test fluid, °C^{-1}; k is the isothermal compression coefficient of the annular test fluid, MPa^{-1}; V_v is the volume of the annular test fluid, m^3; ΔT is the average temperature change in the annulus, °C; Δp is the change in annular pressure, MPa.

By substituting Eq. (17) into Eq. (16), the calculation formula for the annular trapped pressure is obtained as follows:

$$\Delta p = \frac{\alpha}{k}\Delta T - \frac{1}{kV_{\mathrm{v}}}\Delta V_{\mathrm{a}} \tag{18}$$

From Eq. (18), it can be concluded that the annular trapped pressure is closely related to changes in annular volume and temperature increments. Variations at the annular interface lead to fluctuations in annular volume. During testing, both the inner and outer casings of the trapped annuli are subjected to pressure and temperature effects, resulting in changes to the inner and outer diameters of the casing strings. When combined with the thermal expansion and compression of the annular fluid, these factors collectively contribute to variations in annular volume. These effects can be categorized into four primary components [27,28]:

(1) Changes caused by the thermal expansion of the annular test fluid;
(2) Changes caused by the compression of the annular test fluid;
(3) Changes caused by the thermal expansion of the casing;
(4) Changes caused by the compression of the casing.

The radial displacement caused by the thermal expansion of the casing is:

$$u_{h1} = \alpha_c \Delta T_h \frac{(1+u)\left(r_{ho}{}^2 - r_{hi}{}^2\right)}{(1-u)\,2r_{ho}} \tag{19}$$

where, u_{h1} is the radial displacement due to thermal expansion of the casing (where h denotes annulus A, B, and C), m; α_c is the isobaric expansion coefficient of the casing, °C^{-1}; u is the Poisson's ratio of the string, r_{ho} is the outer diameter of the casing, m; r_{hi} is the inner diameter of the casing, m.

The change in annular volume caused by the radial displacement due to thermal expansion of the casing is:

$$\Delta V_{h1} = \pi\left[(r_{\mathrm{ho}} + u_{\mathrm{h1}})^2 - r_{\mathrm{ho}}{}^2\right] L_h \tag{20}$$

where, ΔV_{h1} is the annular volume change caused by the thermal expansion of the casing, m^3; L_h is the length of the annular section, m.

The volume change caused by the thermal expansion of the annular test fluid is calculated using the following equation:

$$\Delta V_{\mathrm{h2}} = \pi\alpha\Delta T_h L_h \left(r_{(\mathrm{h+1})\mathrm{i}}{}^2 - r_{\mathrm{ho}}{}^2\right) \tag{21}$$

where, ΔV_{h2} is the volume change due to the expansion of the annular test fluid, m^3.

The radial displacement of the casing caused by compression under annular pressure can be expressed as:

$$u_{\mathrm{h2}} = \frac{r_{\mathrm{o}}\Delta p\,(1+u)\left[r_{\mathrm{hi}}{}^2 + 2\,(1-2u)\,r_{\mathrm{ho}}{}^2\right]}{E\,(r_{\mathrm{ho}}{}^2 - r_{\mathrm{hi}}{}^2)} \tag{22}$$

where, u_{h2} is the radial displacement of the casing due to compression, m^3; E is the elastic modulus of the casing string, MPa.

The annular volume change caused by the compression of the casing under annular pressure is:

$$\Delta V_{h3} = \pi L_h \left[(r_{ho} + u_{h2})^2 - (r_{ho} + u_{h1} - u_{h2})^2 \right] \tag{23}$$

where, ΔV_{h3} is the volume change caused by the compression of the casing, m^3.

The volume change of the annular test fluid due to compression is:

$$\Delta V_{h4} = \pi k L_h \Delta p \left(r_{(h+1)i}^2 - r_{ho}^2 \right) \tag{24}$$

where, ΔV_{h4} is the volume change due to the compression of the annular test fluid, m^3.

Based on Eqs. (20) and (21), Eqs. (23) and (24), the volume changes of each annulus can be calculated as follows:

$$\Delta V_h = -\Delta V_{h1} + \Delta V_{h2} + \Delta V_{h3} - \Delta V_{h4} \tag{25}$$

where, ΔV_h is the change in annular volume, m^3.

By substituting the volume changes of each annulus into Eq. (18), the annular trapped pressures during the test caused by thermal expansion can be calculated.

3 Example Calculation and Model Verification

To calculate the distribution of annular trapped pressure during the testing period of an offshore high-temperature and high-pressure gas well, a case study is conducted using well Y located in the eastern South China Sea. The known parameters are as follows: the water depth is 1070 m, the depth of the wellbore section below the seabed is 4476 m, the bottom hole temperature is 153°C, and the reservoir pressure is 79 MPa.

The well is a typical four-casing structure, consisting of three annuli. The geometrical parameters of each casing string are summarized as follows:

(1) Conductor casing: inner diameter 34.05 in, outer diameter 36 in, setting depth 1313 m;
(2) Surface casing: inner diameter 18.89 in, outer diameter 20 in, setting depth 1992 m;
(3) Technical casing: inner diameter 12.42 in, outer diameter 13.38 in, setting depth 3331 m;
(4) Production casing: inner diameter 8.34 in, outer diameter 9.63 in, setting depth 4346 m.

Annuli A, B, and C are all sealed annuli, among which the trapped pressure in annulus A can be controlled and released through the subsea test tree and the wellhead. The basic data and related parameters of well Y are shown in Table 1.

Table 1: The basic data and related parameters of well Y

Parameter	Value	Parameter	Value
Poisson's ratio of the casing.	0.3	Geothermal gradient (°C·100 m^{-1})	3.3
Poisson's ratio of the cement sheath.	0.15	Specific heat capacity of natural gas ($J\cdot(kg\cdot°C)^{-1}$)	3800
Poisson's ratio of the stratum	0.24	Stratum density ($g\cdot(cm^3)^{-1}$)	2.15
Convective heat transfer coefficient ($W\cdot(m\cdot°C)^{-1}$)	11,200	Test production ($m^3\cdot d^{-1}$)	100,000

(Continued)

Table 1 (continued)

Parameter	Value	Parameter	Value
Thermal conductivity of the test fluid ($W\cdot(m\cdot°C)^{-1}$)	0.86	Linear expansion coefficient of the casing ($°C^{-1}$)	0.0000182
Seafloor mudline temperature (°C)	4	Thermal conductivity of the stratum ($W\cdot(m\cdot°C)^{-1}$)	1.92
Elastic modulus of the casing (GPa)	210	Thermal conductivity of the casing ($W\cdot(m\cdot°C)^{-1}$)	50.5
Thermal expansion coefficient of the test fluid ($°C^{-1}$)	0.000465	Compressibility coefficient of the test fluid (MPa^{-1})	0.000483

The model was implemented and solved iteratively in MATLAB based on the algorithm illustrated in Fig. 2. The input parameters include wellbore geometry, thermal and mechanical properties of the casing, cement sheath, and formation, as well as the properties of the test fluid, geothermal gradient, and operating conditions. A suitable time step is defined for the simulation to ensure both stability and computational efficiency.

At each time step, the initial trapped pressure or the annular volume change for each annulus (A-C) is assumed, together with a specified convergence tolerance. The radial thermal resistance of each well section is calculated and then used in the heat transfer equations to sequentially determine the tubing temperature, the outer surface temperature of the cement sheath, and the temperature of each annulus, considering thermal coupling effects.

With the updated temperature field, the model computes the corresponding volume changes resulting from casing thermal expansion, fluid thermal expansion, casing compression, and fluid compression. The total annular volume variation is then used in the volume compatibility equation to update the trapped pressure. This process is repeated iteratively using a fixed-point method until both temperature and pressure variations satisfy the convergence criteria. When convergence is achieved, the results of temperature distribution and trapped pressure are recorded and used for model verification and analysis in the subsequent section.

The experimental data used for validation in this study were obtained from laboratory-scale physical simulations of annular pressure buildup in deepwater wells, as reported in reference [29]. In these experiments, fluid samples were placed in a high-pressure autoclave to reproduce the thermal and pressure conditions encountered in deepwater wellbores. The temperature of the trapped annular fluids was gradually increased, and the corresponding pressure changes were recorded to characterize the thermal expansion and pressure buildup behavior. These results provide reliable and representative data for evaluating the accuracy of predictive models.

Based on these experimental data, the average relative error between the calculation results of the model proposed in this paper and the measured data is approximately 6.15%, which meets engineering accuracy requirements. The model also demonstrates rapid and stable convergence.

Compared with existing models that either neglect annular coupling effects or are limited to liquid-phase flow scenarios, the proposed model incorporates temperature–pressure coupling and annular volume deformation under high-temperature, high-pressure gas well conditions. Other models show maximum errors within 13% and an average error of about 7.5%, whereas the proposed model achieves

an average relative error of 6.15%, reflecting an approximate 18% improvement in prediction accuracy. The comparison between the model calculation results and the experimental data is shown in Table 2.

Table 2: Comparison of model calculation results with experimental data

Annular temperature (°C)	Experimental data (MPa)	Model calculation results (MPa)	Relative error (%)
22	25.6	27.33	6.75
44	48.8	46.35	5.02
56	49.4	52.70	6.68

The relative error was calculated using the following formula:

$$\delta = \frac{|P_c - P_e|}{P_e} \times 100\% \tag{26}$$

where, P_c is the model calculation result, MPa; P_e is the experimental data, MPa; δ is the relative error, %.

When the test production is 10×10^4 m^3/d, the temperature variation along the wellbore and the distribution of annular pressure are shown in Fig. 4.

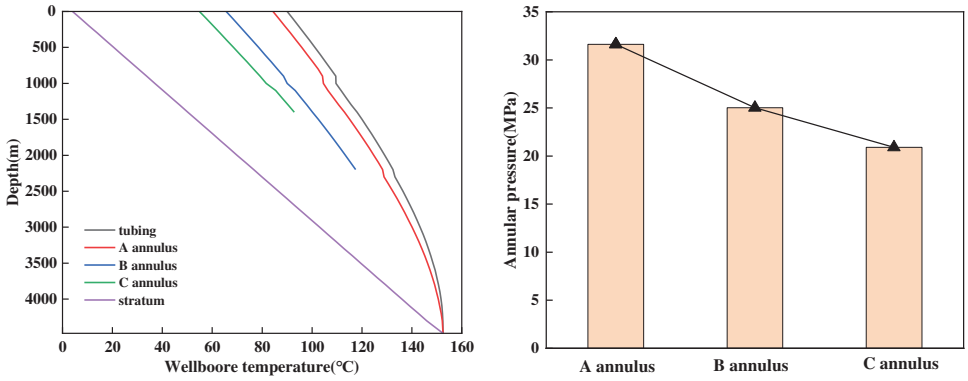

Figure 4: (**a**) The temperature variation of different sections inside the wellbore with depth; (**b**) The pressure distribution of the annulus inside the wellbore

As illustrated in Fig. 4a, the wellbore temperature increases with depth, from the wellhead to the bottom hole. At the wellhead, the temperature distribution from highest to lowest is as follows: fluid inside the tubing, annulus A,annulus B, and annulus C. The temperature differences among the various sections are more pronounced at shallower depths and gradually decrease as the bottom hole is approached.

Fig. 4b shows that at a gas test production of 10×10^4 m^3/d, the trapped pressure in annulus A is higher than in annulus B, with annulus C exhibiting the lowest trapped pressure. Specifically, the trapped pressures in annuli A, B, and C are 31, 25, and 21 MPa, respectively. This distribution is primarily attributed to the fact that annulus A is closest to the tubing. As high-temperature and high-pressure gas flows upward through the tubing during testing, annulus A experiences the greatest temperature increase, resulting in the highest trapped pressure.

4 Analysis of Sensitivity Parameters

During the model solving and verification process, numerous parameters have a critical impact on annular temperature and annular pressure. Therefore, it is necessary to conduct a sensitivity analysis to investigate the influence of different parameters on these responses. Table 3 lists the key parameters considered in the sensitivity analysis, together with their variation ranges and research purposes.

Table 3: Key parameters in the sensitivity analysis

Parameter	Variation range	Purpose in sensitivity study
Testing time (h)	0–20	Thermal response over time
Test production (10^4 m^3/d)	10–120	Effect of production rate on heat transfer and pressure buildup
Geothermal gradient (°C/100 m)	2.0–4.0	Influence of formation temperature distribution
Casing elastic modulus (GPa)	200–300	Impact of casing stiffness on annular volume change
Casing Poisson's ratio	0.1–0.4	Casing deformation characteristics
Thermal expansibility of the annular test fluid ($°C^{-1}$)	2–8 (10^{-4})	Effect of fluid thermal expansibility
Compressibility of the annular test fluid (MPa^{-1})	3–8 (10^{-4})	Effect of fluid compressibility on annular volume response
Well depth (m)	3400–5000	Bottom-hole temperature and pressure conditions
Annular section length (m)	2200–3000	Influence of annular structural geometry

4.1 Testing Time

Fig. 5 shows the variation curves of annular temperature increment and annular pressure with testing time.

As shown in Fig. 5a, the longer the testing time, the greater the temperature increase within the annuli. The temperature trends in annuli A and B are generally similar. Since annulus A is located closest to the tubing, it experiences the highest temperature rise, followed by annulus B, while annulus C shows the lowest temperature increase. Throughout the testing period, the annular temperature distribution from highest to lowest is: annulus A > annulus B > annulus C. The rate of temperature rise is more pronounced during the early stages of testing and gradually slows over time.

This behavior is mainly attributed to the large temperature difference between the high-temperature gas inside the tubing and the initially cooler annular fluid at the start of testing. This temperature contrast drives rapid heat transfer from the tubing to the surrounding annuli. As the test progresses, the annular fluid gradually absorbs heat, which reduces the temperature gradient between the tubing and the annuli. Consequently, the rate of heat transfer decreases, and the temperature rise becomes slower and more gradual.

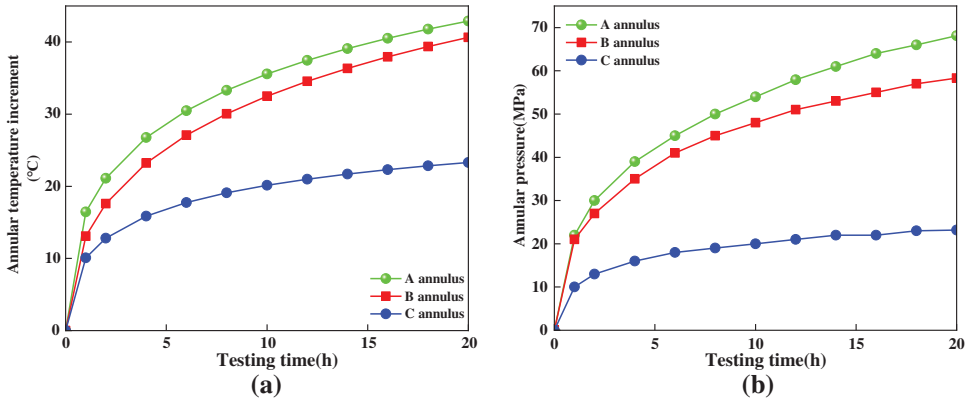

Figure 5: (**a**) The variation of annular temperature increment with testing time; (**b**) The variation of annular pressure with testing time

As shown in Fig. 5b, the annular pressure also increases with testing time. The pressure rise is most pronounced during the early stage but gradually levels off as time progresses. This trend occurs because the thermal resistance of the surrounding formation increases over time. Although the annular fluid continues to absorb heat from the high-temperature gas in the tubing, less heat is lost to the formation. This results in a slower rate of temperature increase within the annulus and, subsequently, a reduced rate of pressure buildup.

Among the three annuli, annulus A experiences the highest trapped pressure, followed by annulus B, while annulus C shows the lowest.

4.2 Test Production

The test production of a gas well is one of the key factors affecting annular temperature and pressure during offshore high-temperature and high-pressure well testing. To analyze the impact of test production on annular temperature and pressure throughout the wellbore, the variations in annular temperature increment and annular pressure under different test productions (with a baseline production rate of 10×10^4 m^3/d) were calculated, as shown in Fig. 6.

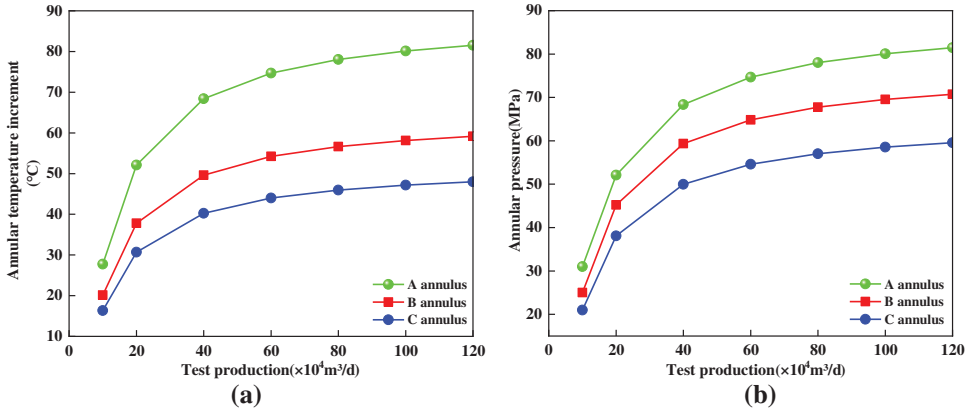

Figure 6: (**a**) The variation of annular temperature increment with test production; (**b**) The variation of annular pressure with test production

As illustrated in Fig. 6a, higher test production results in a greater increase in annular temperature. Under these conditions, annulus A exhibits the highest temperature rise, followed by annulus B, while annulus C shows the lowest. At lower test production rates, changes in annular temperature are more pronounced; however, as production increases, temperature variations tend to stabilize. When the test production reaches 120 × 10^4 m^3/d, the temperature increments in annuli A, B, and C are 54°C, 39°C, and 31°C, respectively.

Fig. 6b further shows that annular pressure also increases with test production. Among the three annuli, annulus A experiences the highest pressure, followed by annulus B, while annulus C maintains the lowest. When the test production is below 40 × 10^4 m^3/d, the pressures in all annuli rise sharply with increasing gas output. Beyond this threshold, however, the rate of pressure increase slows and gradually stabilizes.

For example, as the test production rises from 10 × 10^4 to 40 × 10^4 m^3/d, the pressures in annuli A, B, and C increase sharply from 31, 25, and 21 MPa to 68, 59, and 49 MPa, respectively. This rapid pressure buildup poses significant safety risks to the tubing, wellbore integrity, and the long-term stability of offshore HTHP gas wells.

In summary, gas production volume plays a critical role in determining annular temperature and pressure behavior. Accurately understanding the variation characteristics of annular pressure and temperature with respect to production time and daily output is essential for designing appropriate production systems and ensuring the safe, efficient, and sustainable development of oil and gas resources.

4.3 Geothermal Gradient

Fig. 7 illustrates the relationship between annular temperature increment and annular pressure with respect to the geothermal gradient. As shown in Fig. 7a, the annular temperature exhibits a linear positive correlation with the geothermal gradient—the higher the geothermal gradient, the greater the annular temperature increase. In this analysis, the baseline geothermal gradient is 2.0°C/100 m. Among the three annuli within the wellbore, annulus A shows the highest temperature rise, followed by annulus B, while annulus C records the lowest.

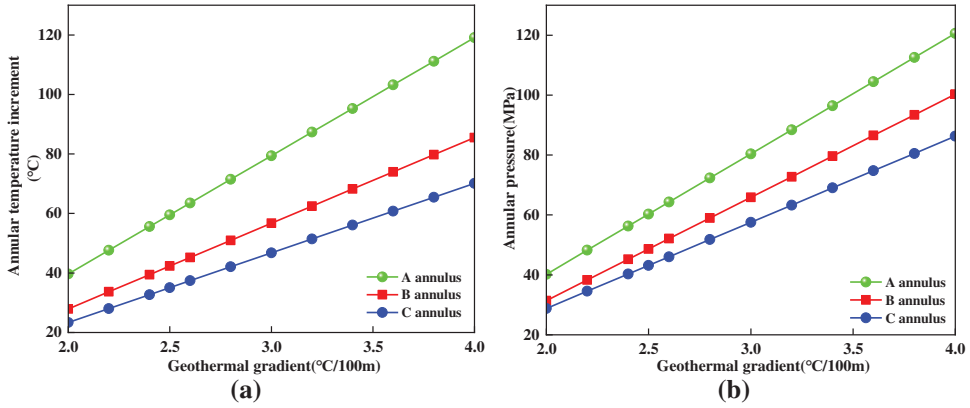

Figure 7: (**a**) The variation of annular temperature increment with geothermal gradient; (**b**) The variation of annular pressure with geothermal gradient

When the geothermal gradient increases from 2.5°C/100 to 4.0°C/100 m, the temperature increment in annulus A rises from 59°C to 119°C; in annulus B, from 42°C to 85°C; and in annulus C, from 35°C to 70°C.

As illustrated in Fig. 7b, annular pressure also increases linearly with the geothermal gradient. The greater the geothermal gradient, the higher the annular trapped pressure. Among the three annuli, annulus A consistently exhibits the highest pressure, followed by annulus B, with annulus C showing the lowest. Specifically, as the geothermal gradient rises from 2.5°C/100 to 4.0°C/100 m, the trapped pressure in annulus A increases from 59 to 118 MPa; in annulus B, from 58 to 117 MPa; and in annulus C, from 46 to 107 MPa. By comparing the slopes of the lines in Fig. 7b, it is evident that the pressure in annulus A increases the fastest, followed by annulus B, while the pressure increase in annulus C is the slowest.

Therefore, during the production testing of high-temperature and high-pressure (HTHP) gas wells, the effects of the geothermal gradient on both annular temperature and pressure should be carefully evaluated. For critical annular sections, such as annulus A, employing thermal insulation measures—such as vacuum-insulated tubing or heat-resistant coatings—can effectively reduce heat transfer from the inner tubing to the outer annuli. This approach slows the temperature increase in the outer annuli and mitigates annular pressure buildup induced by thermal expansion, thereby enhancing wellbore safety and integrity.

4.4 Casing Properties

To investigate the influence of casing elastic modulus and Poisson's ratio on annular pressure during testing of offshore high-temperature and high-pressure gas wells, the test production rate is set at 40 × 10^4 m^3/d, the geothermal gradient at 3.3°C/100 m, and the testing duration at 10 h. The baseline elastic modulus of the casing is 200 GPa. The effect of the casing's elastic modulus on annular trapped pressure is illustrated in Fig. 8.

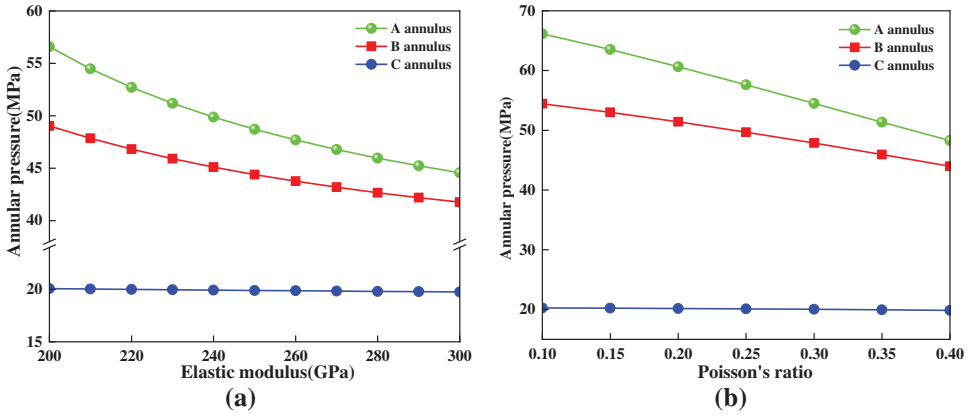

Figure 8: (**a**) The variation of annular pressure with casing elastic modulus; (**b**) The variation of annular pressure with casing Poisson's ratio

As shown in Fig. 8a, increasing the elastic modulus of the casing significantly reduces the trapped pressures in annuli A and B, while the pressure in annulus C remains almost unchanged. When the elastic modulus increases from 210 to 300 GPa, the trapped pressure in annulus A decreases sharply from 56.58 to 44.56 MPa, representing the largest drop. In annulus B, the pressure declines from 49.04

to 42.76 MPa, though at a slower rate than in annulus A. In contrast, annulus C shows only a slight reduction—from 20.06 to 19.70 MPa—indicating low sensitivity to changes in elastic modulus.

Fig. 8b illustrates how the trapped pressure varies with the casing's Poisson's ratio. As Poisson's ratio increases, annular pressures gradually decrease. Among the three annuli, annulus A experiences the most pronounced and rapid pressure drop, followed by annulus B, while annulus C exhibits minimal variation in both magnitude and rate.

Because the model accounts only for deformation of the inner casing, changes in elastic modulus and Poisson's ratio strongly influence its volumetric deformation. As a result, the trapped pressures in annuli A and B are highly sensitive to variations in casing mechanical properties. In contrast, annulus C, positioned between the intermediate and surface casings, is less affected because it undergoes minimal volume change from inner casing deformation.

This behavior can be explained by the mechanical response of the casing material. When modeled as a plastic body, an increase in elastic modulus or Poisson's ratio enhances the casing's resistance to thermal expansion and compression, thereby reducing volumetric deformation. This reduction creates more available space within the annulus for fluid expansion. Consequently, under the same temperature rise, casings with higher elastic modulus and Poisson's ratio can effectively mitigate annular pressure buildup.

Therefore, in the structural design of wellbores, selecting casing materials with relatively high elastic modulus and Poisson's ratio is beneficial for mitigating annular trapped pressure and ensuring well integrity under high-temperature and high-pressure conditions, particularly in the most critical annular space A, where the use of high-grade steel such as P110 casing is recommended.

4.5 Physical Properties of the Annular Test Fluid

The thermal expansibility and compressibility of the annular test fluid are also key factors influencing annular trapped pressure. In this study, the baseline values of the isothermal expansion coefficient and the isothermal compressibility coefficient of the annular test fluid are 2×10^{-4} °C^{-1} and 3×10^{-4} MPa^{-1}. As shown in Fig. 9a, a higher thermal expansion coefficient of the annular test fluid leads to an increase in annular trapped pressure. Among the three annuli, annulus A exhibits the most rapid pressure increase, followed by annulus B, while annulus C shows the slowest rate of pressure rise. This is because, under identical temperature conditions, a higher thermal expansion coefficient causes greater volumetric expansion of the fluid, thereby resulting in a more significant pressure buildup.

Fig. 9b presents the variation in annular pressure with respect to the compressibility of the test fluid. As the compressibility increases, the annular trapped pressure decreases. Annuli A and B are more significantly affected by changes in compressibility, while annulus C shows relatively minor variation. This is because higher compressibility allows the fluid to undergo greater volume reduction under pressure, thereby better accommodating thermal expansion and mitigating the rise in annular pressure.

Therefore, it is recommended to employ foam cement slurry or other highly compressible, low-expansion cement systems during the cementing process. These materials can effectively moderate the rate of annular pressure increase in well sections subjected to significant temperature variations, thereby reducing the risk of annular trapped pressure buildup and improving overall wellbore integrity.

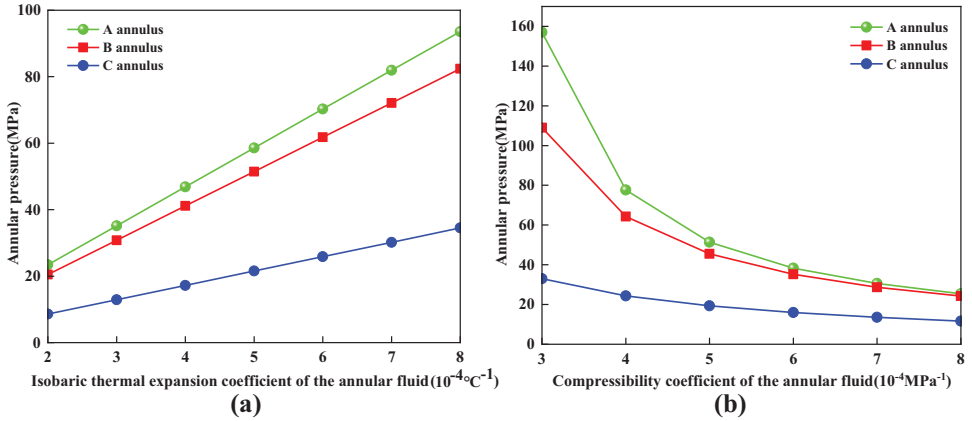

Figure 9: (**a**) The variation of annular pressure with the isobaric thermal expansion coefficient of the test fluid; (**b**) The variation of annular pressure with the compressibility coefficient of the test fluid

4.6 Well Depth

The influence of well depth on annular temperature and trapped pressure is primarily manifested through changes in bottom hole temperature. When the test production is 120 × 10^4 m^3/d, the variations in annular temperature and pressure under different well depths are analyzed, as shown in Fig. 10.

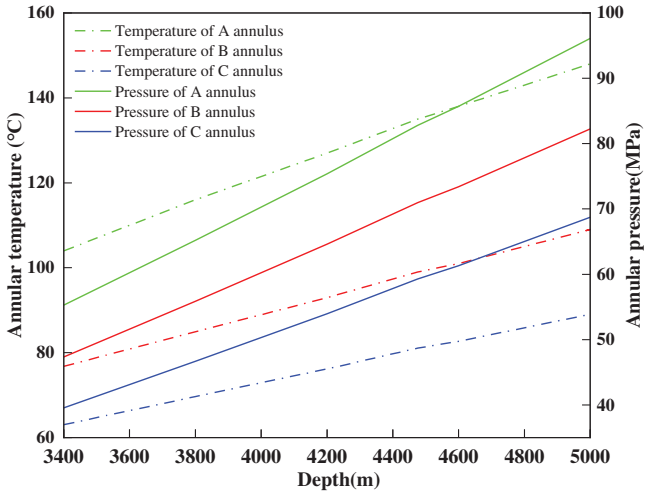

Figure 10: The variation of annular temperature and annular pressure with well depth

The figure shows that the temperatures in annuli A, B, and C all increase with greater well depth. Among them, annulus A has the highest temperature, followed by annulus B, while annulus C exhibits the lowest.

As the well depth increases from 3400 to 5000 m, the temperature in annulus A rises from 104°C to 148°C—an increase of 44°C. In annulus B, the temperature increases from 76°C to 109°C, a rise of 33°C; while in annulus C, it increases from 63°C to 89°C, an increase of 27°C. The slopes of the temperature curves indicate that the temperatures in annuli A and B are more sensitive to depth

changes, while the temperature in annulus C is relatively less affected. This difference reflects the varying degrees of thermal influence among the annuli.

Because annular pressure trends closely follow the temperature variations, the trapped pressure also increases with well depth. According to the pressure curve slopes, annuli A and B show a more pronounced rise in pressure with increasing depth, whereas annulus C maintains the lowest pressure and is the least affected by depth variations.

4.7 Length of the Annular Section

To investigate the influence of annular section length on annular temperature and trapped pressure, the test production is set at 120 $\times 10^4$ m^3/d, and the length of the B annular section is varied. The resulting changes in temperature and trapped pressure for each annulus are calculated and presented in Fig. 11. The results show that the annular temperatures and trapped pressures in annuli A, B, and C remain nearly unchanged despite variations in the length of the B annular section. Therefore, it can be concluded that the length of the annular section has no significant effect on either annular temperature or trapped pressure.

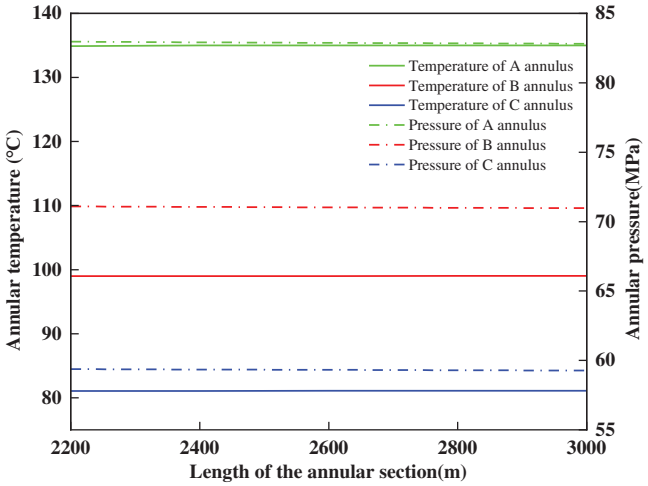

Figure 11: The variation of annular temperature and annular pressure with the length of the B annular section

5 Conclusions

(1) This paper conducts a systematic theoretical study on annular trapped pressure induced by thermal effects. By integrating the PVT equation of state and the principle of volume compatibility, it investigates the impact of temperature and volume changes in each annulus during well testing on trapped pressure. A predictive model for annular trapped pressure during high-temperature and high-pressure offshore gas well testing is established, enabling forecasting of annular temperature and trapped pressure throughout the testing period.

(2) A numerical simulation study of annular temperature and annular trapped pressure was carried out based on the high-temperature and high-pressure Y well case in the eastern South China Sea. The simulation results show that the average relative error between the model calculation results and the experimental data is approximately 6.15%. When the gas test production is 10 $\times$ 10^4 m^3/d, the trapped pressures in annuli A, B, and C are 31, 25, and 21 MPa, respectively.

As the test production increases to 120×10^4 m^3/d, the average temperature in annulus A rises by 54°C, while the temperature increases in annuli B and C are slightly lower, at 39°C and 31°C, respectively. The annular pressures also show a significant upward trend.

(3) Sensitivity analysis results indicate that the rise in annular temperature and trapped pressure mainly occurs at the early stages of testing. With increased testing time and test production, annular temperature and trapped pressure initially rise and then gradually stabilize. The annular trapped pressure is linearly and positively correlated with geothermal gradient, the expansion coefficient of annular fluid, and well depth, while it shows a negative correlation with the casing's elastic modulus, Poisson's ratio, and the compressibility of the annular fluid.

(4) This study provides theoretical support for parameter optimization, annular pressure risk evaluation, and wellbore integrity analysis during high-temperature and high-pressure gas well testing. In future research, systematic indoor physical simulation experiments can be further conducted. These experiments should fully consider actual wellbore structure, formation fluid properties, gas-liquid ratio, etc., and establish corresponding formation annular trapped pressure prediction models to enhance the applicability and prediction accuracy of the models.

Acknowledgement: Not applicable.

Funding Statement: The Production and Research Projects of Shenzhen Branch of CNOOC "Research on Key Technologies for Drilling and Completion of HTHP Wells in the Eastern South China Sea" (No. SCKY-2023-SZ-18).

Author Contributions: The authors confirm contribution to the paper as follows: methodology, visualization and supervision: Zhihua Rao; writing—original draft, conceptualization: Kunxiang Liu; validation, data curation: Bin Chen; formula analysis: Yao You; writing—review & editing: Qiang Zhang; investigation: Yang Jiao; resources, methodology: Baobo Liu; scientific research consultant, technical support: Miao He. All authors reviewed the results and approved the final version of the manuscript.

Availability of Data and Materials: Data available on request from the authors.

Ethics Approval: Not applicable.

Conflicts of Interest: The authors declare no conflicts of interest to report regarding the present study.

References

1. Dong G, Chen P. A review of the evaluation methods and control technologies for trapped annular pressure in deepwater oil and gas wells. J Nat Gas Sci Eng. 2017;37:85–105. doi:10.1016/j.jngse.2016.11.042.
2. Zhang B, Xu Z, Lu N, Liu HT, Liu JQ, Hu ZQ, et al. Characteristics of sustained annular pressure and fluid distribution in high pressure and high temperature gas wells considering multiple leakage of tubing string. J Petrol Sci Eng. 2021;196(1):108083. doi:10.1016/j.petrol.2020.108083.
3. Zhang Z, Xiang S, Yuan Z, Tang H. A coupling prediction model of annular pressure build-up for deepwater oil and gas wells during transient-state testing. Geoenergy Sci Eng. 2023;230(2):212162. doi:10.1016/j.geoen.2023.212162.
4. Kan C, Yang J, Yu X, Wang Y. A novel mitigation on deepwater annular pressure buildup: unidirectional control strategy. J Petrol Sci Eng. 2018;162:577–87. doi:10.1016/j.petrol.2017.10.072.

5. Cao L, Sun J, Zhang B, Lu N, Xu Y. Analysis of multiple annular pressure in gas storage well and high-pressure gas well. Energy Eng J Assoc Energy Eng. 2023;120(1):35. doi:10.32604/ee.2022.022867.
6. Simon F, Frêne J. Analysis for incompressible flow in annular pressure seals. J Tribol. 1992;114(3):431–8. doi:10.1115/1.2920902.
7. Wang X, Pang X, Xian M, Sun B, Wang Z, Ren Y, et al. Numerical study on transient annular pressure caused by hydration heat during well cementing. Appl Sci. 2022;12(7):3556. doi:10.3390/app12073556.
8. Wang J, Dong X, Gao D. Trapped annular pressure caused by thermal expansion between double packers in ultra-deep wells. In: International Conference on Computational & Experimental Engineering and Sciences. Cham, Switzerland: Springer Nature; 2024. p. 220–30. doi:10.1007/978-3-031-68775-4-16.
9. Zhang B, Guan Z, Lu N, Hasan AR, Wang Q, Xu B. Trapped annular pressure caused by thermal expansion in oil and gas wells: a review of prediction approaches, risk assessment and mitigation strategies. J Petrol Sci Eng. 2019;172:70–82. doi:10.1016/j.petrol.2018.09.041.
10. Xie R, Zhang L. A new prediction model of annular pressure buildup for offshore wells. Appl Sci. 2024;14(21):9768. doi:10.3390/app14219768.
11. Wang LS, Gao B, Gao L, Hu T. Prediction of annular pressure caused by thermal expansion by considering the variability of fluid properties. Appl Therm Eng. 2018;141:234–44. doi:10.1016/j.applthermaleng.2018.05.110.
12. da Veiga AP, Martins IO, Barcelos JGA, Ferreira MVD, Alves EBDM, da Silva AK, et al. Predicting thermal expansion pressure buildup in a deepwater oil well with an annulus partially filled with nitrogen. J Petrol Sci Eng. 2022;208:109275. doi:10.1016/j.petrol.2021.109275.
13. Ding L, Rao J, Xia C. Transient prediction of annular pressure between packers in high-pressure low-permeability wells during high-rate, staged acid jobs. Oil Gas Sci Technol. 2020;75(1):49. doi:10.2516/ogst/2020046.
14. Liu J, Song X, Zhang Z, Ding J, Ding Y. Prediction method for annular pressure buildup in deepwater wells based on fluid solid phase deposition. Processes. 2025;13(3):890. doi:10.3390/pr13030890.
15. Maiti S, Gupta H, Vyas A, Kulkarni SD. Evaluating precision of annular pressure buildup (APB) estimation using machine-learning tools. SPE Drill Compl. 2022;37(1):93–103. doi:10.2118/196179-PA.
16. Ding L, Li S, Lian Z, Wei Z, Qi J, Tang Z. Modeling and prediction of sustained casing pressure of high-pressure and high-temperature gas wells during production operations. SPE J. 2025;30(5):2372–87. doi:10.2118/225420-PA.
17. Wu Y, Zhou J, Yang J, Zhang TW, Zou X, Zhang XQ, et al. Research on wellbore integrity assurance technology for deepwater high-pressure oil and gas wells. Energies. 2023;16(5):2230. doi:10.3390/en16052230.
18. Wang H, Zhang H, Li J, Sun T. Study on annular pressure buildup phenomenon in subsea wells considering the effect of cement. Energy Sci Eng. 2022;10(1):81–95. doi:10.1002/ese3.1008.
19. Wang H, Li M, Zhao Q, Hao W, Zhang H, Li Y, et al. Study on casing safety evaluation in high-temperature wells with annular pressure buildup. Processes. 2023;11(7):1915. doi:10.3390/pr11071915.
20. Yu X, Gao Y, Zhao X, Zhou Y. Research on prediction of A-annular pressure buildup of deepwater gas wells at the initial stage of production. In: Sun B, Sun J, Wang Z, Chen L, Chen M, editors. Proceedings of the Fifth International Technical Symposium on Deepwater Oil and Gas Engineering, DWOG-Hyd 2023. Vol. 472. Singapore: Springer; 2024. p. 28–39. doi:10.1007/978-981-97-1309-7_3.
21. Hasan R, Izgec B, Kabir S. Sustaining production by managing annular-pressure buildup. SPE Prod Oper. 2010;25:195–203. doi:10.2118/120778-PA.
22. Zhang B, Zheng Y, Deng J, Lu N, Cao L, Wang Q, et al. Modeling analysis of the temperature profile and trapped annular pressure induced by thermal-expanded liquid in a deep gas well. Front Phys. 2022;10:1014842. doi:10.3389/fphy.2022.1014842.
23. Wang G, Li W, Xiang Y, Wang YF, Liu YH, Liu JT, et al. Deepwater oil and gas well annulus pressure management strategy. Chem Technol Fuels Oils. 2024;60(3):629–38. doi:10.1007/s10553-024-01721-x.

24. Wang H, Zhang H, Li J, Chen A, Liu J, Sun T, et al. Study on annular pressure buildup in offshore heavy oil thermal recovery wells considering dissolved gas contained in annuli. Energies. 2021;14(11):3213. doi:10.3390/en14113213.
25. Zeng J, Kou BB, Liu H, Yu Y, Li J, Li B, et al. Coupling effect of annular volume change and non-linear fluid thermal property on annular pressure buildup in multi-layer annuluses of deepwater well. Arab J Geosci. 2022;15(10):931. doi:10.1007/s12517-022-10090-w.
26. Martins IO, da Silva AK, Silva ECCM, Hasan AR, Barbosa JR Jr. Predicting the annular pressure behavior during water injection in offshore wells with a transient, multiphysics model. J Petrol Sci Eng. 2022;218:110992. doi:10.1016/j.petrol.2022.110992.
27. Li C, Guan Z, Zhang B, Cao LH, Xu ZX, Xie JF, et al. Analysis of tubing-casing annular pressure in early production stage in high temperature high pressure wells. In: Proceedings of the Offshore Technology Conference Asia; 2020 Nov 3–6; Kuala Lumpur, Malaysia. OTC-30059-MS. doi:10.4043/30059-MS.
28. Zhang B, Sun B, Deng J, Lu N, Zhang Z, Fan HJ, et al. Method to optimize the volume of nitrogen gas injected into the trapped annulus to mitigate thermal-expanded pressure in oil and gas wells. J Nat Gas Sci Eng. 2021;96:104334. doi:10.1016/j.jngse.2021.104334.
29. Williamson R, Sanders W, Jakabosky T, Serio M, Griffith JE. Control of contained-annulus fluid pressure buildup. In: Proceedings of the SPE/IADC Drilling Conference; 2003 Feb 19–21; Amsterdam, The Netherlands. SPE-79875-MS. doi:10.2118/79875-MS.